New Leaky Surface Waves in Anisotropic Metal-Diffused Optical Waveguides

KAZUHIKO YAMANOUCHI, TOSHIAKI KAMIYA, AND KIMIO SHIBAYAMA

Abstract—**Propagation of guided waves in anisotropic metal-diffused optical waveguide is investigated. Two-dimensional guide-mode dispersion curves are computed and classified for a metal-diffused waveguide with arbitrary optic-axis orientation in various diffusion depth. It is found that a new leaky surface wave exists in the region where the refractive index is above the cutoff value, not below it. Typical values of decay constant are about 5 dB/cm for the wave propagating along X axis on 128° rotated Y-cut $LiNbO_3$, and 35 dB/cm for the wave propagating along the direction making an angle of 70° to X axis on Y-cut plane $LiNbO_3$. We were able to observe the leaky surface waves experimentally.**

I. Introduction

RECENT INTEREST in electro-optic acousto-optic thin film waveguides and metal-diffused waveguides [1], [2] for the fabrication of modulators [3], switches [4], and other optical thin film devices [5] in integrated optics has prompted the theoretical investigation of wave propagation in anisotropic thin film and metal-diffused waveguides. Wave propagation in anisotropic thin films with arbitrary crystal axis has been investigated by many workers [6], [7]. On the other hand, as for optical waves in metal-diffused materials, the wave propagations only in some special propagation directions on some special crystal cuts, e.g., the optical waves propagating along crystal axis in the surface normal to crystal axis, have been investigated.

This paper presents a theoretical and experimental study of optical waves in arbitrary direction of metal-diffused waveguides in which the substrate may be uniaxial material. Some of the special features of the dispersion and field distributions for anisotropic metal-diffused waveguides are described herein. The value of the extraordinary refractive index of uniaxial crystal varies with the propagation direction. Therefore, the guided modes that contain extraordinary wave components have directional dependency, and convert to new leaky surface waves in certain propagation directions, radiating energy into a substrate [8]–[10]. It is also found that the field distributions in anisotropic waveguide differs greatly from that of isotropic wave guides. For example, the direction of the field exists almost in parallel with crystal optic axis.

II. Theoretical Analysis

Solution of the guided mode in metal-diffused waveguides can be obtained by the Wentzel–Kramer–Brillouin [11] or the differential numbered solution (DNS) [5] method if the optical waves propagate along crystal axis in the surface normal to the other crystal axis. However, these methods cannot be used for waves which propagate in arbitrary directions of anisotropic crystals. To get solutions for such waveguides a multilayer approximation is applied, as shown in Fig. 1.

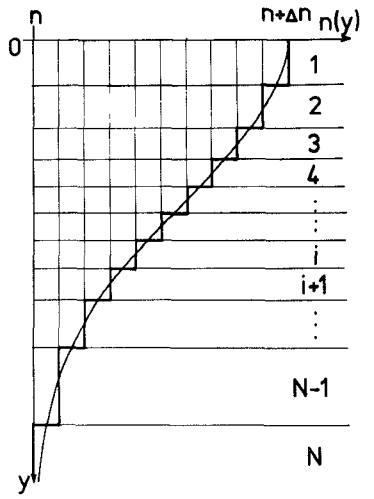

Fig. 1. Multilayer-approximation method.

Letting the dielectric waveguide material occupy the half-space, the dielectric constants below the surface of the metal-diffused crystal are approximated by

$$\epsilon_{11}(x_2)=\epsilon_{22}(x_2)=\epsilon_o+\Delta\epsilon_o \exp\left[-\left(\frac{x_2}{D}\right)^2\right]$$

$$\epsilon_o=n_o^2\epsilon_v, \qquad \Delta\epsilon_o=2n_o\Delta n_o\epsilon_v \quad (1)$$

$$\epsilon_{11}(x_2)=\epsilon_e+\Delta\epsilon_e \exp\left[-\left(\frac{x_2}{D}\right)^2\right]$$

$$\epsilon_e=n_e^2\epsilon_v, \qquad \Delta\epsilon_e=2\Delta n_e n_e\epsilon_v \quad (2)$$

where ϵ_v is the dielectric constant of vacuum and ϵ_o and ϵ_e are the ordinary and extraordinary dielectric constants, respectively. The graded variation of dielectric constants in (1) and (2) are approximated by N layers with uniform dielectric constant in each layer, as shown in Fig. 1.

Harmonic electromagnetic propagation is described by the Maxwell equations

$$\nabla\times\boldsymbol{E}=-j\omega\mu\boldsymbol{H} \quad (3)$$

$$\nabla\times\boldsymbol{H}=j\omega\epsilon_v\cdot\bar{\epsilon}\cdot\boldsymbol{E} \quad (4)$$

in which $\bar{\epsilon}$ is a symmetric 3×3 matrix with real components $\epsilon_{em}=\epsilon_{me}$ in an anisotropic waveguide.

We assume the electromagnetic fields of each layer to

Manuscript received May 4, 1977; revised December 28, 1977.

The authors are with the Research Institute of Electrical Communication, Tohoku University, Sendai, Japan.

0018-9480/78/0400-0298$00.75

be

$$(E_{x_k})_i = \sum_{m=1}^{2} A^{(m)} \alpha_k^{(m)} \exp\left[P_k(m) x_2 + j(n_{\text{eff}} k_0 x_1 - \omega t)\right],$$

$$k = 1,2,3 \quad \text{and} \quad x_1 = x, \quad x_2 = y, \quad x_3 = z \qquad (5)$$

where $\alpha_k^{(m)}$ is a component of the normalized eigenvector corresponding to a lower half-plane root $P_k^{(m)}$ and the propagation vector in the surface is specified by its projections n_{eff} on the x_1 axis. These total electromagnetic fields are substituted into boundary conditions

$$(E_{x_k})_i = (E_{x_k})_{i+1} \qquad (H_{x_k})_i = (H_{x_k})_{i+1}$$

$$(k = 1,3). \qquad (6)$$

The boundary condition equation, obtained from (6) is

$$|D(i,j)| = 0, \qquad i,j = 1,2 \cdots. \qquad (7)$$

The determinant is calculated for successive values of parameter n_{eff}, until the complex determinant of the coefficients of (7) is rendered equal to zero within a certain predetermined accuracy. The corresponding values of the weighting factors $A^{(m)}$ can then be determined from (7). No combination of crystal, free surface, and direction of propagation was found for which a solution satisfying the boundary conditions could not be obtained by the preceding iterative procedure, i.e., multilayer approximation. In some special cases, the surface-wave solution degenerates or becomes very close to a bulk wave solution; i.e., one of the decay constant in x_2-direction $P^{(2)}$ approaches or becomes equal to zero while the corresponding coefficient $A^{(2)}$ dominates the other one. In such degenerate or near-degenerate cases n_{eff} becomes complex; that is $k = k_0 n_{\text{eff}}(1 + j\delta)$, where δ is the decay constant in x_1-direction per wavelength. It means the optical wave is no more a guided wave but a leaky surface wave which propagates along the surface radiating some acount of energy into substrate.

III. Analytical and Numerical Results

A. Approximation Approach

First, we shall discuss the precision of multilayer approximation of anisotropic graded index waveguides. One example of the result is shown in Table I, where Y-cut X-propagation $LiNbO_3$ is employed, and $\Delta n_e = \Delta n_o = \Delta n = 0.01$ and layer-number $N = 10$. Consulting with Table I, it is evident that the multilayer approximation gives precise values comparable with the WKB or the DNS method.

B. Rotated Y-Cut X-Propagation $LiNbO_3$

Permitivity-tensor components ϵ_{im} for a rotated Y-cut shown in Fig. 2 are given by

$$\begin{bmatrix} \epsilon_{11} & 0 & 0 \\ 0 & \epsilon_{22} & \epsilon_{23} \\ 0 & \epsilon_{32} & \epsilon_{33} \end{bmatrix}. \qquad (8)$$

$LiNbO_3$ single crystals have a negative uniaxial index, and their values of refractive index are $n_o = 2.286$, $n_e = 2.20$ for ordinary and extraordinary waves, respectively.

Fig. 3 shows the dispersion curve versus the diffusion depth D in the case of $\Delta n_e = \Delta n_o = 0.01$ and the polar angle

TABLE I
Effective Refractive Indices n_{eff} Compared with Multilayered, the WKB, and the DNS Method, $\Delta n_e = \Delta n_o = 0.01$ and $N = 10$

D	Mode	Our method n_{eff}	D.N.S. n_{eff}	WKB n_{eff}
3.0	0	2.20583	2.20581	2.20577
	1	2.20160	2.20159	2.20155
	0	2.20738	2.20734	2.20735
5.0	1	2.20430	2.20426	2.20426
	2	2.20187	2.20184	2.20184
	3	2.20027	2.20028	2.20027

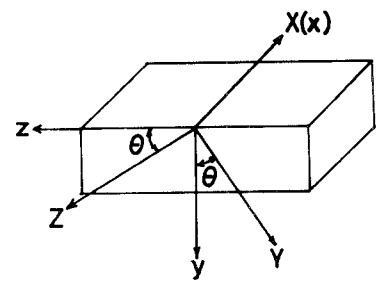

Fig. 2. Relation between crystal axis and optical wave propagation on rotated Y-cut crystal. X, Y, Z indicate principal crystal axis; X, Y, Z are Cartesian coordinate for the analysis.

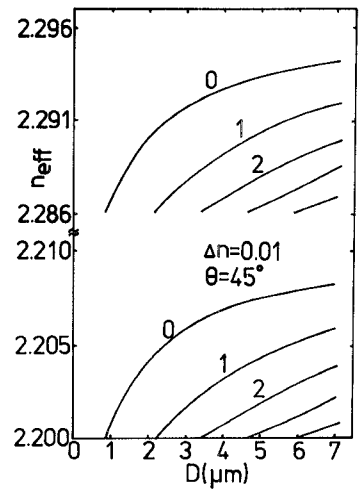

Fig. 3. Dispersions versus diffusion depth D in the case of $\Delta n = \Delta n_e$, $\Delta n_o = 0.01$, and $\theta = 45°$.

$\theta = 45°$. The waves between $n_{\text{eff}} = 2.286$ and 2.296 are the guided modes. On the other hand, the waves between $n_{\text{eff}} = 2.20$ and 2.21 are the leaky surface waves, which differ from leaky waves existing below $n_{\text{eff}} = 2.20$. The decay constants δ (dB/cm) of the leaky surface waves due to radiation of energy at $\theta = 45°$ are shown in Fig. 4 as a function of diffusion depth D. The δ is about 2~4 (dB/cm) at $D = 4$ μm and 10 dB/cm at $D = 1$ μm. The values of n_{eff} and δ of the leaky surface waves versus θ at $D = 5$ μm are shown in Figs. 5(a) and 5(b). The δ shows the maximum value at $\theta = 45°$ where ϵ_{23} is at its largest value.

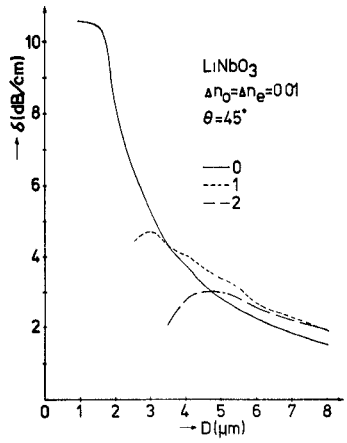

Fig. 4. Decay constants δ (dB/cm) of leaky surface waves versus D at $\theta = 45°$.

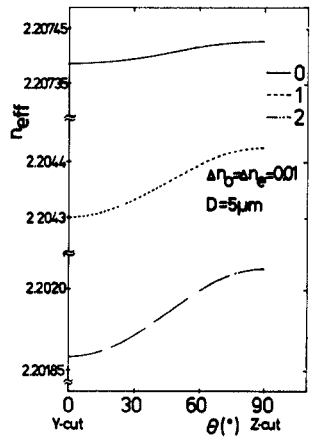

(a)

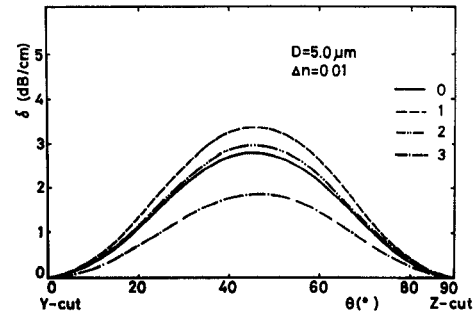

(b)

Fig. 5. (a) Dispersion curves of effective refractive index n_{eff} versus θ and (b) decay constants δ versus θ at $D = 5$ μm.

Figs. 6(a) and 6(b) show the electric field distributions of the guided mode and the leaky surface mode at $\theta = 127.86°$. Amplitude of the guided mode decreases exponentialy as the depth from the surface increases. On the other hand, that of the leaky surface mode oscilliates on an exponential function and has bulk wave components. We can see that direction of the electric fields nearly agrees with the crystal axis; i.e., the directions of the electric fields of the guided mode and the leaky mode exist in parallel with the Z axis and the Y axis of the crystals, respectively.

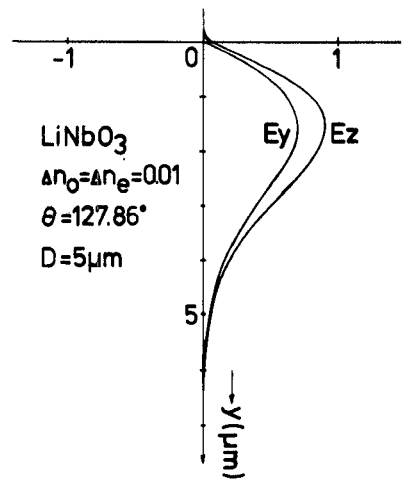

(a)

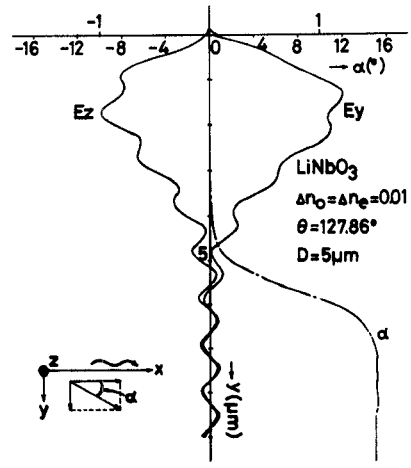

(b)

Fig. 6. Electric field distribution versus depth Y at $\theta = 127.86°$. (a) Guided mode. (b) Leaky surface mode.

The leaky surface waves radiate power into substrate. We cannot, therefore, calculate the total power by integrating the power flow from zero to infinite of the depth. However, we can calculate the power density as a function of depth from the surface. Fig. 6(b) also shows the azimuth angle of the Poynting vector form the crystal surface. Near the surface, the direction of the Poynting vector is parallel to the surface, the same as the guided waves. However, at about six wavelengths below the surface, the bulk term is the only term left in the solution, and the direction of the Poynting vector is titled 15° from the surface.

C. Propagation on the Y-Cut Plane of $LiNbO_3$

Permitivity tensors for the Y-cut plane are written as

$$\begin{bmatrix} \epsilon_{11} & 0 & \epsilon_{13} \\ 0 & \epsilon_{22} & 0 \\ \epsilon_{13} & 0 & \epsilon_{33} \end{bmatrix}. \tag{9}$$

The anisotropic wave equation provides an algebraic equation of the fourth order.

Fig. 7 shows the coordinate system and the direction of

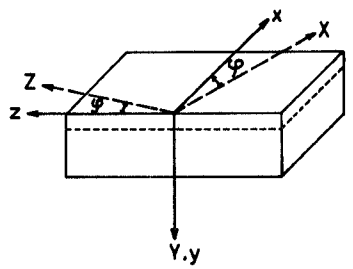

Fig. 7. Relation between crystal axis and optical wave propagation on *Y*-cut plane.

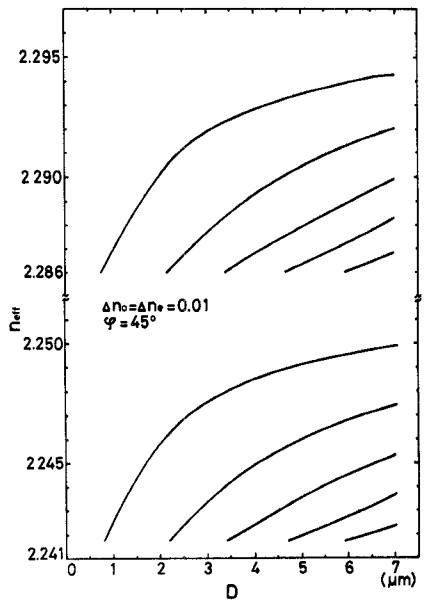

Fig. 8. The n_{eff} versus D at $\Delta n=\Delta n_e=\Delta n_o=0.01$ and $D=5$ μm.

wave propagation. The wave, which is a TM-guided mode at $\varphi=0°$, remains a guided mode even if angle φ is not equal to zero. On the other hand, the wave, which is a TE-guided mode at $\varphi=0°$, becomes the leaky surface mode by an increasing angle φ. Fig. 8 shows the dispersion curves versus D at $\varphi=45°$ on the Y-cut plane and for $\Delta n_o=\Delta n_e=0.01$. The waves of $n_{eff}=2.286\sim2.296$ are guided modes, while the waves of $n_{eff}=2.2418\sim2.250$ are leaky surface modes. The n_{eff} of the leaky surface waves change with the azimuth angle φ in the Y-cut plane. Fig. 9 shows the decay constant δ of the leaky surface waves versus φ for $\Delta n_e=\Delta n_o=0.01$ and $D=5$ μm. The δ increases as φ increases. However, when the n_{eff} becomes greater than the ordinary refractive index of the substrate $n_o=2.286$, the leaky modes convert to guided modes. Therefore, the decay constant δ is reduced to zero. These values of φ where the leaky modes are converted to the guided modes are $\varphi=73.4°$ for 0 mode, $\varphi=77.8°$ for 1 mode, and $\varphi=81.8°$ for 2 mode, respectively.

Figs. 10(a) and 10(b) show the field distribution and direction of the Poynting vector α of the leaky surface waves at $\varphi=20°$ and $\varphi=70°$. The oscillatory component E_y at $\varphi=20°$ is much smaller than at E_y at $\varphi=70°$. These correspond to the values of the decay constant $\delta=2$ dB/cm at $\varphi=20°$ and $\delta=35$ dB/cm at $\varphi=70°$, respectively.

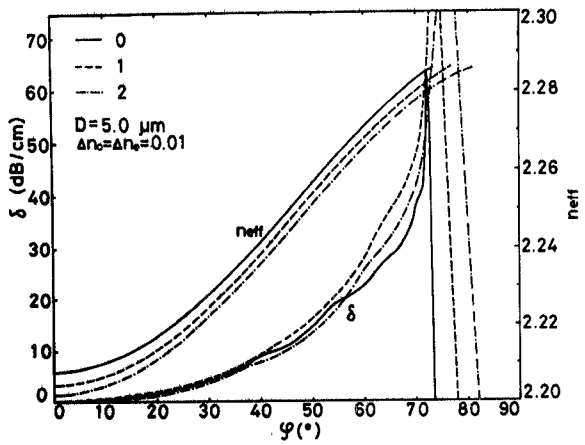

Fig. 9. The decay constant δ and effective refractive index n_{eff} of the leaky mode versus the φ at $\Delta n=\Delta n_e=\Delta n_o=0.01$ and $D=5$ μm. The effective refractive indices greater than the ordinary refractive index of the substrate are not shown because they become complicated due to mode coupling. Details of the dispersion curves are shown in Fig. 11.

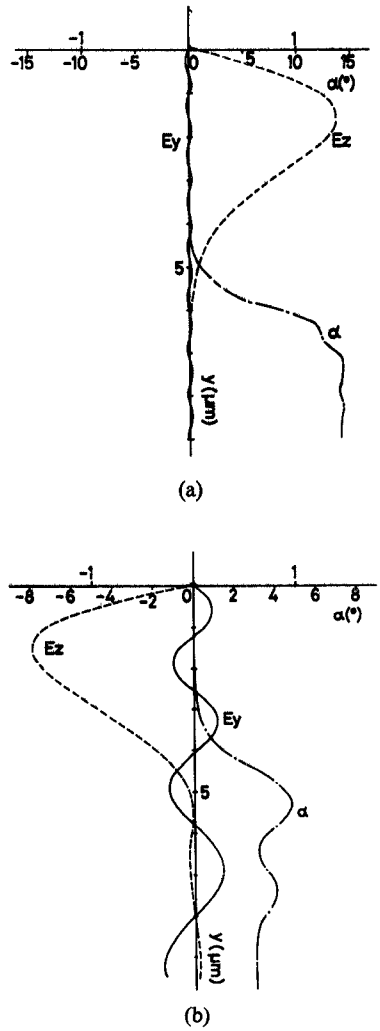

Fig. 10. Electric field distributions and direction of Poynting vector α versus depth from the surface Y. (a) $\varphi=20°$; (b) $\varphi=70°$.

Table II shows the δ and α_∞ for the depth far from the surface at $\varphi=70°$. These values will be compared later with the experimental values.

Fig. 11 shows the dispersion curve versus φ from 60° to 90°. As φ increases, the TM mode component of the

TABLE II
THE δ AND THE α_∞ AT $\varphi=70°$

Mode	δ (dB/cm)	α_∞ (°)
0	35	3°
1	42	4.3°
2	49	5.0°

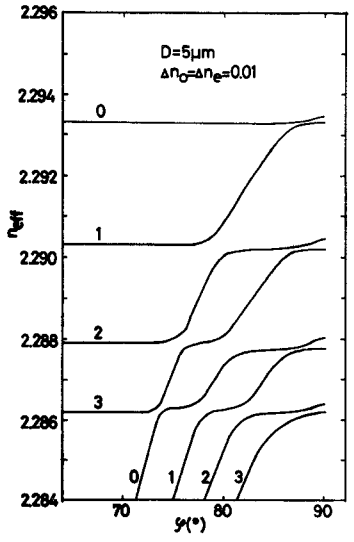

Fig. 11. Dispersion curves versus φ from 60° to 90°.

quasi-TE mode (pure TE mode at $\varphi=0°$) increases and n_{eff} approaches to the n_{eff} of the quasi-TM mode until, at a certain angle, the TM component of the quasi-TE mode becomes equal to the TE component. When n_{eff} of the quasi-TE mode passes through 2.286, the leaky surface wave becomes the guided mode, as shown previously. In this figure, mode switching from quasi-TE mode to quasi-TM mode occurs at about $\varphi=85°$ to TM_0–TE_0, $\varphi=80°$ to TM_1–TE_0, etc. Further information of mode switching is obtained by examining the actual polarization for the waveguide modes.

Figs. 12(a) and 12(b) show the electric field distribution for two waveguide modes (the quasi-TE mode and quasi-TM mode) of Fig. 11 at $\varphi=73.5°$. Roughly speaking, the polarizations are seen as being nearly circular, rotating in opposite directions, for the two modes. The situation is very similar to that of propagation along the optic axis of uniaxial, optically active crystals such as quartz and $Bi_{12}SiO_{20}$.

If linear polarization enters this type of crystal, it is split into two circular polarizations which, after traveling a distance d within the crystal, will be shifted in the relative phase by

$$\Delta=\frac{2\pi d}{\lambda_0}\delta n. \tag{10}$$

On recombining, the two circular polarizations will yield a linear polarization after rotating by $\Delta/2$ rad with respect to the incident polarization. In the present metal-diffused waveguide, we consequently expect that any incident linear polarization will be rotated through $\pi/2$ after a distance

$$d=\frac{\lambda_0}{2\delta n}. \tag{11}$$

The conversion distance d is 2.0 mm for TM_0-TE_3 at 73.5 shown in Fig. 11.

IV. Physical Explanation of Leaky Surface Waves

Now let us explain why leaky surface waves exist in an anisotropic metal-diffused waveguide. When the propagation direction coincides with the crystal axis, pure TE and TM modes propagate independently. But in the other case, ordinary and extraordinary waves propagating in a layer with the extraordinary index $n_e+\Delta n_e$ and the ordinary index $n_o+\Delta n_o$ are coupled due to reflection at the crystal surface. The refractive index of $LiNbO_3$ is $n_o>n_e$. For a confined optical wave propagation, the effective refractive index of wave should be between n_o and $(n_o+\Delta n_o)$, and n_e and $(n_e+\Delta n_e)$. A wave between n_o and $(n_o+\Delta n_o)$ is usually a guided mode, because n_{eff} is larger than n_o and n_e. On the other hand, a wave between n_e and $(n_e+\Delta n_e)$ has a large electric field vector in the direction of the extraordinary refractive index and a small value in that of the ordinary one, and these two components couple at the crystal surface. Since the n_{eff} is smaller than the n_o of the substrate, the field component in the direction of the ordinary index passes through the boundary to the substrate. The wave between n_e and $(n_e+\Delta n_e)$, therefore, becomes a leaky surface mode. The above discussion can be applied to other materials such as $LiTaO_3$.

V. Experimental Results

The fabrication of metal-diffused optical waveguides by diffusion of Ti and Ni films into $LiNbO_3$ substrates has been studied by Kaminow *et al.* [1]. The optical waveguides had excellent optical qualities. With Ti film of 500Å diffused at 1050°C for 7 h, waveguides were obtained on a rotated 128° Y-cut plane of $LiNbO_3$.

The guiding experiments of the 128° rotated Y-cut X-propagation $LiNbO_3$ are performed by using a 56° rutile prism-metal diffused layer coupler and an He–Ne laser $\lambda_0=6328$ Å, as illustrated in Fig. 13. Two modes are observed in the guided waves and three modes are observed in the leaky surface waves.

Table III shows the observed and theoretically calculated values of the n_{eff}. To deduce observed n_{eff}, the refractive indices of the rutile prism, $n_o=2.583$ and $n_e=2.863$ were used. We could not observe the leaky components because of the small values of δ (dB/cm); however, the observed n_{eff} nearly agreed with theoretical ones.

As for the Y-cut plane of $LiNbO_3$, guiding experiments are performed on the waves propagating along the directions with angles of 0°, 30°, 45°, and 70° to the X axis. These speciments are fabricated by depositing the Ti film of 500 Å and diffusing it at 1050°C for 7 h. The optical waves are excited by the same rutile prism as shown in Fig. 13.

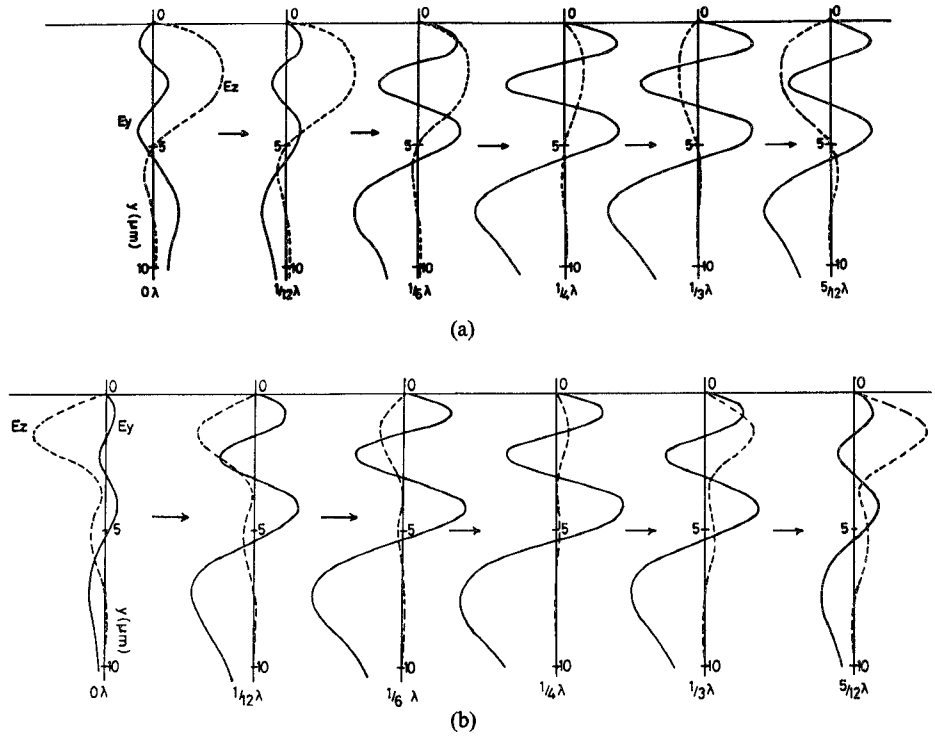

Fig. 12. Electric field distribution for the two waveguide modes.

TABLE III
OBSERVED AND CALCULATED VALUES OF n_{eff}

m	Observed	Calculated
0	2.214	2.208
1	2.210	2.204
2	2.207	2.202

m	Observed	Calculated
0	2.292	2.292
1	2.289	2.289

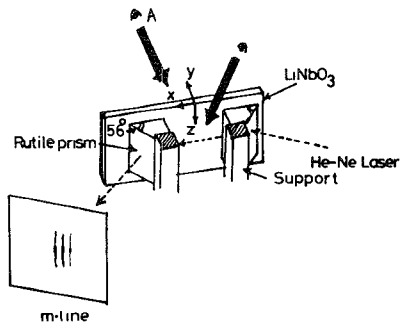

Fig. 13. Experimental configuration.

Table IV shows the n_{eff} of the guided modes and the leaky surface modes at $\varphi=45°$. The theoretical values are calculated by $\Delta n_e=\Delta n_o=0.01$ and $D=5$ μm. Agreement between the observed and the theoretical values are within 2 parts in 100.

TABLE IV
THE n_{eff} OF THE GUIDED MODES AND THE LEAKY SURFACE MODES AT $\varphi=45°$

Mode	m	Observed (n_{eff})	Calculated (n_{eff})
Leaky	0	2.250	2.2491
	1	2.248	2.2460
	2	2.246	2.2436
Guided	0	2.293	2.2934
	1	2.290	2.2904
	2	2.288	2.2880
	3	2.287	2.2863

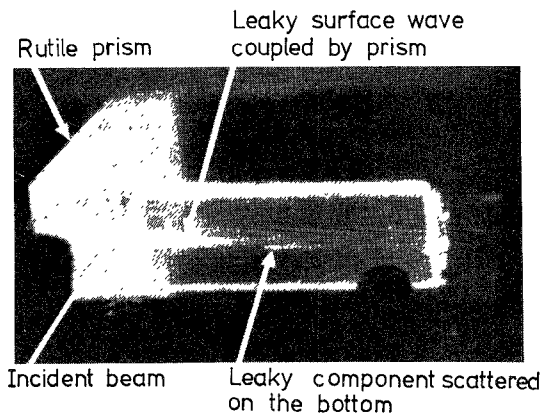

Fig. 14. Streak of 0-mode leaky surface wave at $\varphi=45°$.

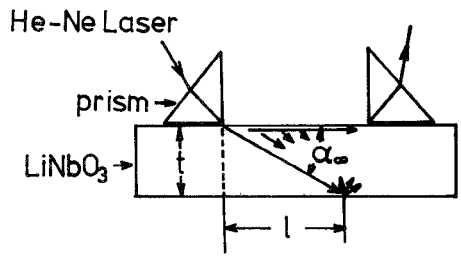

Fig. 15. Radiating angle α_∞. The α_∞ corresponds to the α far from the surface in Fig. 10.

TABLE V
OBSERVED AND THE CALCULATED VALUES OF α_∞ (a) $\varphi=45$; (b) $\varphi=70°$

ϕ	m	Observed α_∞(°)	Calculated α_∞(°)
45°	0	10.2°	10.3°
	1	10.7°	10.7°
	2	11.2°	11.1°
70°	0	4.7°	3.0°
	1	5.2°	4.3°
	2	5.6°	5.0°

Fig. 14 shows a streak of the leaky surface wave of the 0 mode at a 45° angle, viewed from point A in Fig. 13. The streak near the input prism at the top surface is a guiding component, and the streak of the middle of $LiNbO_3$ at the bottom surface is a leaky component. As brightness of the guiding component decreases, that of the leaky component decreases.

The radiating angle α_∞ is determined by (12), as shown in Fig. 15.

$$\tan \alpha_\infty = \frac{t}{l}. \tag{12}$$

Table V(a) shows the observed and the theoretical values of α_∞. The observed and theoretical values are in good agreement.

Fig. 16 shows streaks of the leaky surface waves at a 70° angle and for 0, 1, 2 modes. Table V(b) shows the observed and calculated values of the radiating angle α_∞ for 0, 1, 2 modes. From these results, we are able to confirm the leaky surface waves.

VI. Conclusion

We analyzed anisotropic metal-diffused optical waveguides and we found new leaky surface waves. It has been shown that the direction of the electric field vector nearly agrees with the principal crystal axis. TE–TM mode conversion occurs at a certain angle. Since the metal-diffused waveguides have excellent optical qualities, mode conversion effect will be useful for a practical device. Finally, we were able to confirm leaky surface waves by experiments.

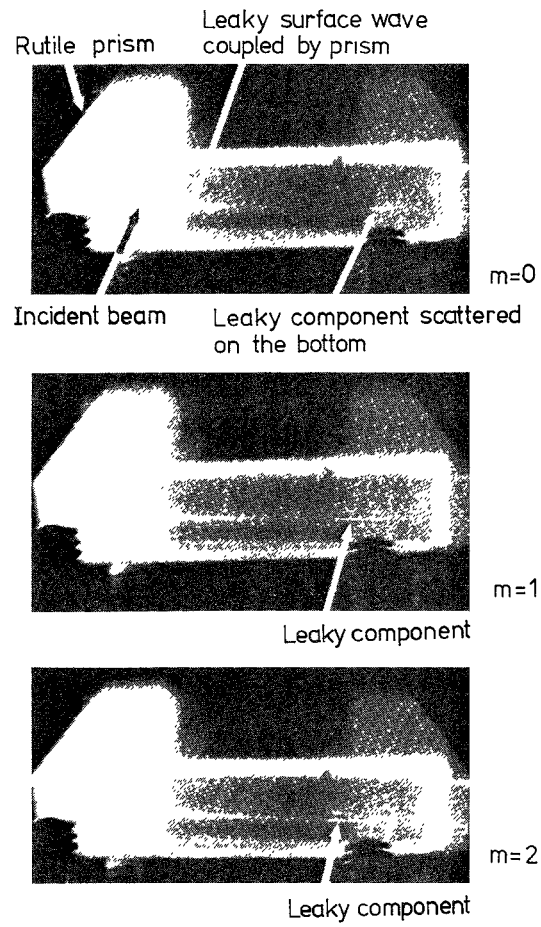

Fig. 16. Streaks of the leaky surface waves at $\varphi=70°$. (a) 0 mode. (b) 1 mode. (c) 2 mode.

Acknowledgment

The authors wish to thank M. Yasumoto for his help in calculation of the leaky surface wave.

References

[1] R. V. Schmidt and I. P. Kaminow, "Metal-diffused optical waveguides in $LiNbO_3$," *Appl. Phys. Lett.*, vol. 25, pp. 458–460, Oct. 1974.

[2] I. P. Kaminow and J. R. Carruthers, "Optical waveguiding layers in $LiNbO_3$ and $LiTaO_3$," *Appl. Phys. Lett.*, vol. 22, pp. 326–328, Apr. 1973.

[3] C. S. Tsai, "Wideband guided-wave acoustooptic Bragg-devices and applications," in *Proc. IEEE Ultrasonics Sym.* (Los Angels, CA) pp. 120–123, Sept. 1975.

[4] I. P. Kaminow, V. Ramaswamy, R. V. Schmidt, and E. H. Turner, "Lithium niobate ridge waveguide modulator," *Appl. Phys. Lett.*, vol. 24, pp. 622–624, June 1974.

[5] K. Yamanouchi, K. Higuchi, and K. Shibayama, "TE-TM mode conversion by interaction between elastic surface waves and a laser beam on a metal-diffused optical waveguide," *Appl. Phys. Lett.*, vol. 28, pp. 75–77, Jan. 1976.

[6] D. P. Gia Russo and J. H. Harris, "Wave propagation in anisotropic thin-film optical waveguides," *J. Opt. Soc. Amer.*, vol. 63, pp. 138–145, Feb. 1973.

[7] M. S. Kharusi, "Uniaxial and biaxial anisotropy in thin-film optical waveguides," *J. Opt. Soc. Amer.*, vol. 64, pp. 27–35, Jan. 1974.

[8] S. Adachi, "Study on the guiding mechanism of whistler radio waves," *Radio Sci.*, vol. 69 D, pp. 493–502, Apr. 1965.
[9] T. C. Lim and G. W. Farnell, "Character of psuedo surface waves on anisotropic crystals," *J. Acoust. Soc. Amer.*, vol. 45, pp. 845–851, Apr. 1969.
[10] A. Takayanagi, K. Yamanouchi, and K. Shibayama, "Piezo-electric leaky surface wave in $LiNbO_3$," *Appl. Phys. Lett.*, vol. 17, pp. 225–227, Sept. 1970.
[11] D. Marcuse, "TE modes of graded-index slab waveguides," *IEEE J. Quantum Electron.*, vol. QE-9, pp. 1000–1006, Oct. 1973.

Analysis of Intermodulation Noise in Frequency Converters by Volterra Series

RICHARD B. SWERDLOW, MEMBER, IEEE

Abstract—**Frequency converters produce intermodulation noise in the desired signal band which may be a serious problem for communications systems using amplitude modulation. In this paper, we introduce the Volterra series with time-varying kernels to treat intermodulation in frequency converters with one two-terminal nonlinearity. The method gives exact results up to the order calculated (third order here) for any nonlinearity expressable as a power series, will treat frequency dependence in the nonlinearity as well as the terminations, and leads to a convenient algorithm for computer calculation. The mathematics provides a physical picture of intermodulation of a specific order as being produced by the modulation of lower order products through the nonlinearity. In fact, the solution for a given order of intermodulation currents or charges is the solution of a set of linear equations where the driving functions are intermodulation currents of lower order.**

A program has been written for the specific but important case of an abrupt junction varactor upconverter. Results for an upconverter that might be used for single-sideband operation in the common carrier microwave band show that the largest contribution to intermodulation comes from currents which are at the sum and difference frequencies of the input (IF) signal, corresponding to currents above the input port in frequency and currents in the bias circuitry.

This paper documents previously unpublished work (1972) done as part of the exploratory study of single-sideband modulation on long-haul microwave radio transmission.

I. Introduction

AT LEAST four distinct procedures have been used to calculate the intermodulation distortion of upconverters. Anderson and Leon [1] computed bounds on the intermodulation distortion by an approximate solution to the integral equation describing the converter. Perlow and Perlman [2] related gain compression of a single tone to the magnitudes of distortion products from two tones. Schwarz and Nelson [3] assumed current flow at input, output, pump, and bias circuitry and solved for the intermodulation by substituting into a power series for the diode nonlinearity. Gardiner and Ghobrial [4] express the charge as a series in auxilliary functions which can be found from a set of first-order differential equations. Rice [5] has related this procedure to solution by the Volterra series.

In the present method, the solution is found as a time-varying Volterra series [6]. The first term of the series leads to the linear theory of frequency converters similar to that of Penfield and Rafuse [7]. Thus the formulae and computer algorithms found here are applicable to all types of frequency converters: upconverters to upper and lower sidebands, upconverters with idlers, the equivalent down-converters and parametric amplifiers. The basic limitation is to two-terminal nonlinearities. Formulae developed here are valid for a nonlinear resistance and capacitance in series or the dual situation of parallel nonlinear conductance and inductance. Any linear time-invariant termination is permitted at any frequency where currents may flow; indeed, an important conclusion is that for an upconverter suitable for heterodyne repeaters in the 6-GHz common-carrier band, currents at the sum and difference frequencies of the IF are the substantial contributors to third-order intermodulation distortion at the output. No attempt is made to find analytic solutions to the intermodulation. A strength of the analysis is that it results in an algorithm well-suited to computer calculation; namely, sets of linear equations. The Volterra kernels found permit calculation of gain compression, intermodulation due to multitone inputs, and noise inputs.

II. Circuit to be Studied

Fig. 1 is a schematic representation of an upconverter using a diode as the nonlinearity. The nonlinearity is two terminal and this analysis is restricted to this case; more than one independent current flowing through nonlinearities would require a multidimensional Volterra series. Thevinen's and Norton's theorems were used to lump the linear portion of the circuit, which includes the bias, pump, output, etc., into the two-terminal impedance as

Manuscript received May 9, 1977; revised October 14, 1977.
The author is with Bell Laboratories, North Andover, MA 01845.

0018-9480/78/0400-0305$00.75